A decoupling control strategy for wind turbine blades equipped with active flow controllers

Terence Macquart[1], Alireza Maheri[2] and Krishna Busawon[2]

[1] ACCIS—Advanced Composites Centre for Innovation and Science, University of Bristol, Bristol, UK
[2] Faculty of Engineering and Environment, Northumbria University, Newcastle upon Tyne, UK

ABSTRACT

The use of active controls has shown to be of substantial help in supporting the increasing size of wind turbines by reducing peak stresses and fatigue loads. In this respect, this paper proposes the use of intuitive frequency-based control strategies for reducing loads in wind turbine blades equipped with multi-input multi-output (MIMO) active flow controllers. For that purpose, a loop-shaping approach is considered for analysing the dynamic of actively controlled wind turbine blades. Preliminary aeroelastic simulations are carried out to validate the results. It is shown that the MIMO vibration control problem can effectively be decomposed into a number of decoupled single-input single-output control problems because of the strong correlation between the dominant aeroelastic blade dynamics and actuator deployments. As a result, it is demonstrated that classical single-input single-output control systems can perform as efficiently as MIMO controllers for damping the aeroelastic dynamics of wind turbine blades.

KEYWORDS

aeroelastic control; load reduction; loop-shaping; trailing edge flap; microtab; WTAC

1. INTRODUCTION

It is a well-known fact that the increasing aspect ratio of aerodynamic surfaces such as aircraft wings and rotor blades results in greater loads and structure flexibility. Employing active controls in order to ensure stability, limiting stress peaks and reducing the fatigue experienced by wind turbine blades, has therefore gained significant research interest over the last decade.[1–3] Spanwise and local flow controls have been proposed for controlling the vibrations of aeroelastic structures.[4–6] Spanwise controls are generally very effective but require substantial actuation energy and rapid dynamics that may wear excessively on actuators.[7–10] In comparison, local flow controllers such as control surfaces (CSs) are small and rapid devices distributed along the blades in order to provide control over the local aerodynamic forces.[11–13] This research focuses on the design of control systems and control strategies for wind turbine blades equipped with multiple CS.

The load reduction capabilities of wind turbine blades equipped with CSs is an active field of research.[1,2,6,11,14–17] Amongst the many aeroelastic closed-loop control architectures that have been proposed in order to damp loads employing CSs, the classical control laws [e.g. proportional (P), proportional–derivative (PD) and proportional–integral–derivative (PID)][18–20] and frequency-weighted controllers [e.g. linear quadratic regulator (LQR), linear quadratic Gaussian and model predictive control][6,9,21] are the most commonly employed. In general, current research follows the idea that increasingly complex control architectures such as optimal, multi-input multi-output (MIMO) and predictive control systems will outperform classical controllers.[9,22] However, issues related to the tuning, sensing and state estimation required for MIMO state-based controllers are rarely considered.[9,21,23] Furthermore, it is known that the efficiency and stability of complex model-based control structures may be very sensitive to uncertainty.[21] By contrast, the dynamic system analysis carried out during this research reveals vibratory patterns, which led us to design simple yet effective and robust control systems for load reduction.

The aim of the present research is twofold: (i) to demonstrate that these vibratory patterns can be used to effectively decompose the MIMO vibration control of wind turbine blades into a set of decoupled single-input single-output (SISO) control problems and, as a result, (ii) to show that well-established classical SISO control systems can perform as efficiently as MIMO controllers for damping the aeroelastic dynamics of blades. These are achieved through the modelling, analysis and detailed explanations of the aeroelastic behaviour of wind turbine blades equipped with CSs. Additionally, the obtained results are validated with aeroelastic simulations of a wind turbine case study.

The rest of this paper is structured as follows. In Section 2, the vibration control of wind turbine blades employing CSs is defined as a loop-shaping problem. The general aeroelastic modelling is detailed in Section 3. The aerodynamic models of CSs are presented in Section 4. The load reduction case study is presented and evaluated in Section 5. Finally, Section 6 summarizes the outcomes of this research.

2. A LOOP-SHAPING APPROACH TO LOAD REDUCTION

Figure 1 is a typical representation of an aerostructural system where the plant (P_L), which stands for the wind turbine blade equipped with CSs, is excited by external forces. As for practical applications, these forces are rarely known in advance. Hence, the controller cannot be positioned directly between the plant and the external forces (i.e. feed-forward control). Instead, the forces driving the aeroelastic vibrations are generally alleviated by feedback control as shown in Figure 2.

The load reduction control of wind turbine blades is defined as the alleviation, by means of a control system, of specific aerostructural dynamics excited by external loads. Figure 3 shows the frequency response of an open-loop and an ideally controlled aeroelastic system. In this figure, $1P$ and $2P$ stand for the frequencies to be alleviated. Frequencies $1N$ and $2N$

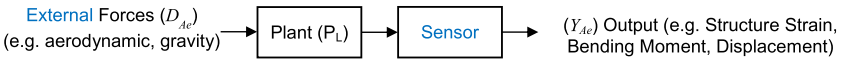

Figure 1. Representation of an open-loop wind turbine (plant) subject to external forces.

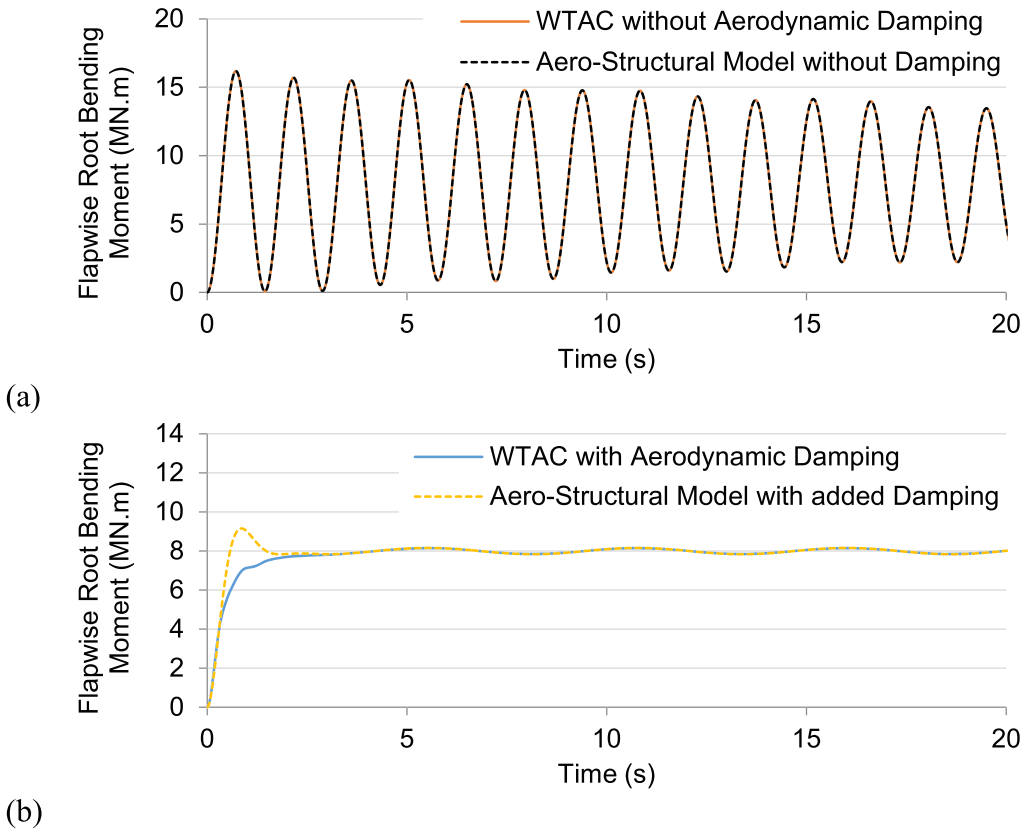

Figure 2. Closed-loop control system of a wind turbine equipped with CSs.

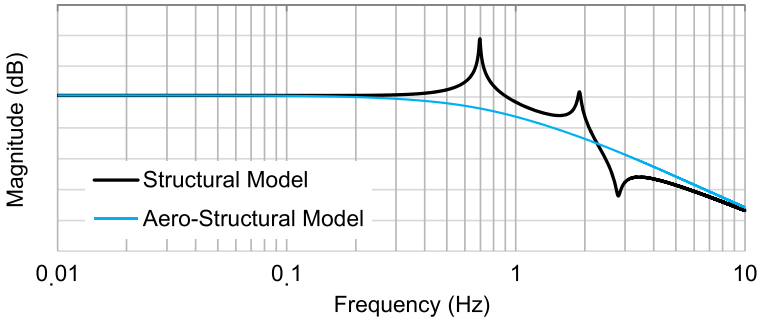

Figure 3. Frequency response of an ideally controlled wind turbine blade for load alleviation.

denote the first and second natural frequencies. An ideal control system shapes the frequency response such that the frequencies to be alleviated are fully damped. Moreover, an ideal controller does not interact with other frequency bandwidths (i.e. $\Delta_f \rightarrow 0$). In other words, the ideal control system behaves like perfect notch filters. The idea of using a control system in order to shape the frequency response of a system is referred to as loop-shaping. While previous studies have demonstrated the effectiveness of this approach for SISO wind turbine blade load alleviation,[24,25] the present study will show that this approach can also be extended to the control of multiple CSs (i.e. MIMO).

While digital or electrical notch filters can achieve substantial attenuation level, there are physical constraints imposed on electro-mechanical devices (i.e. CSs) that limit their loop-shaping capabilities. Moreover, notch filters introduce significant phase shift near the attenuated frequency bandwidths, which in turn may reduce the closed-loop system stability. Neglecting these two limitations when designing control systems is likely to result in poor trade-offs between performance and stability.[21] In other words, the differences between the ideal and achieved frequency shapes can vary significantly as illustrated in Figure 4. One critical advantage of the frequency-based analysis (i.e. loop-shaping) over the time domain control approaches is the ability to clearly explain and visualize the impact of proposed control strategies on the overall aeroelastic dynamic of blades. As a result, effective control systems dedicated to the vibration control of wind turbine blades can be designed. This approach is adopted during the present investigation.

3. BLADES EQUIPPED WITH FLOW CONTROLLERS

The dynamic response of an aerodynamic surface subjected to external forcing is generally obtained by numerical approximation, for which finite element (FE) modelling is one of the dominant approaches. In this research, we use the FE model that we previously developed in Macquart and Maheri[23] and which approximates the aeroelastic behaviour of wind turbine blades using beam elements. Since the large size of FE models is often cumbersome to work with, we use a modal reduction in order to reduce the FE model by conserving only the prime dynamics.[26] Modal approximation with relatively few modes is common for analysing large wind turbine blades dynamics and design control laws.[9,27] In the linear case, the modal reduction results in a series of independent equations that corresponds to the natural frequencies and their respective mode shapes. Denoting the modal coordinate vector $\rightarrow Q$, the aerodynamic surfaces' general modal form is given as

$$M_q \ddot{\vec{Q}} + D_q \dot{\vec{Q}} + K_q \vec{Q} = \vec{F}_q \tag{1}$$

where M_q, D_q and K_q are the equivalent modal matrices for mass, damping and stiffness and $\rightarrow F_q$ is the modal force vector. Rewriting equation (1) in a state space form while conserving only the two primary modes (i.e. high aspect ratio) and

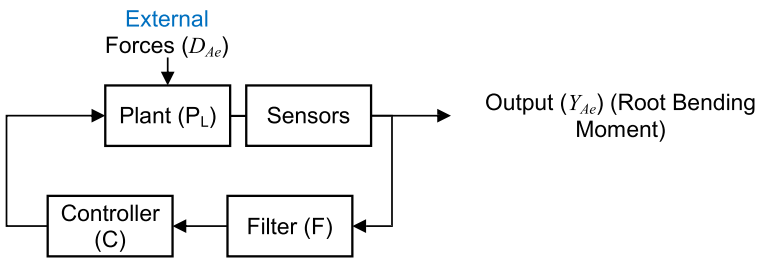

Figure 4. Frequency response of a controlled aeroelastic structure with physical limitations.

coupling the resulting system with the generic flow controllers aerodynamic model (subscript Fc), we obtain the aeroelastic system (subscript Ae) as follows:

$$\dot{\vec{X}}_{Ae} = A_{Ae}\vec{X}_{Ae} + B_{Ae}\,\vec{u} + \vec{D}_{Ae} \tag{2}$$

$$\begin{bmatrix} \dot{Q}_2 \\ \dot{Q}_1 \\ \ddot{Q}_2 \\ \ddot{Q}_1 \\ \dot{\vec{X}}_{Fc} \end{bmatrix} = \begin{bmatrix} 0 & 0 & 1 & 0 & 0 \\ 0 & 0 & 0 & 1 & 0 \\ r_2 & 0 & s_2 & 0 & T_{As2} \\ 0 & r_1 & 0 & s_1 & T_{As1} \\ 0 & 0 & 0 & 0 & A_{Fc} \end{bmatrix} \begin{bmatrix} Q_2 \\ Q_1 \\ \dot{Q}_2 \\ \dot{Q}_1 \\ \vec{X}_{Fc} \end{bmatrix} + \begin{bmatrix} 0 \\ 0 \\ 0 \\ 0 \\ B_{Fc} \end{bmatrix} \vec{u} + \begin{bmatrix} 0 \\ 0 \\ F_{q2} \\ F_{q1} \\ 0 \end{bmatrix} \tag{3}$$

The external force, included into the vector D_{Ae}, on each element is assumed to be a uniformly distributed time varying force. These include aerodynamic forces calculated by an aerodynamic blade element momentum code and gravitational and inertia forces.[28] Since the aerodynamic effects of CSs are generally much greater than their impacts on structural properties, the structural properties are assumed to remain unchanged. As can be observed in equation (3), in open-loop, the CSs are independent from the structure dynamics. On the other hand, the two first modes can be controlled, through T_{As1} and T_{As2}, by the aerodynamic forces generated by the CSs. The deployment of CSs is regulated by the control input vector $\vec{u}$ and the control matrix B_{Fc}. The general form of the output matrix is given as

$$\vec{Y}_{Ae} = C_{Ae}\vec{X}_{Ae} = \begin{bmatrix} c_{11} & c_{12} & 0 & 0 & 0 \\ c_{21} & c_{22} & 0 & 0 & 0 \\ c_{31} & c_{32} & 0 & 0 & 0 \\ . & . & . & . & . \\ . & . & . & . & . \\ c_{N1} & c_{N2} & 0 & 0 & 0 \\ 0 & 0 & 0 & 0 & C_{Fc} \end{bmatrix} \begin{bmatrix} Q_2 \\ Q_1 \\ \dot{Q}_2 \\ \dot{Q}_1 \\ \vec{X}_{Fc} \end{bmatrix} \tag{4}$$

where the N first outputs are typical linear combinations of modal coordinates. By default, these outputs would be the blade displacements resulting from FE analysis. It is also possible to relate the blades displacements, moment and strains based on available blade sensors. The last output line corresponds to the CSs deployment position sensors. Details about blade sensors are given in Section 5.

4. CONTROL SURFACE AERODYNAMIC MODEL

The term CS refers to a subcategory of active flow controllers that control the flow through localized geometric changes. Two promising CSs, namely, trailing edge flaps (TEFs) and microtabs (MTs), are investigated in this study. This section presents the aerodynamic response models of TEFs and MTs. Both CSs are assumed to deploy continuously. Previous work by Macquart and Maheri[23] has shown that while discontinuous controllers can be used for load alleviation, discontinuous controllers tend to increase the CS actuators' wear.

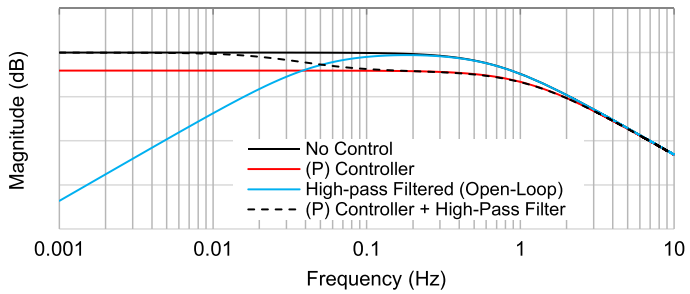

Figure 5. MT ($_{MT}$) and TEF ($_{F}$) normalized aerodynamic responses to a step input ($_{U}$).

4.1. MICROTAB

The typical aerodynamic response of an MT deploying on the pressure side of an aerofoil is shown in Figure 5. The MT aerodynamic model can be divided into two dynamics[29]: (i) a rapid dynamic occurring simultaneously to the MT deployment and (ii) a much slower dynamic during which the flow reaches a steady state. Research by Chow *et al.*[30] has shown that the MT dynamic response also features a delay and an inverse response. However, these dynamics, because of their small amplitudes and short transient existences, are negligible.[29,30] The general MT dynamic response model is described in a state space form as follows:

$$\dot{\vec{X}}_{MT} = A_{MT}\vec{X}_{MT} + B_{MT}u \tag{5}$$

$$\dot{\vec{X}}_{MT} = \begin{bmatrix} 0 & 1 & a_{MT} \\ b_{MT} & c_{MT} & d_{MT} \\ 0 & 0 & \tau_{MT} \end{bmatrix} \vec{X}_{MT} + \begin{bmatrix} 0 \\ 0 \\ 1 \end{bmatrix} u \tag{6}$$

$$\vec{X}_{MT} = \begin{bmatrix} \Delta C_L & \Delta \dot{C}_L - r_{MT}\Delta C_{Lss} & \delta_{MT} \end{bmatrix}^T \tag{7}$$

where, in the state vector, $\vec{X}_{MT}$, ΔC_L and $\Delta C_{L,ss}$ respectively denote the dynamic and steady state lift generated because of the normalized MT deployment height represented by δ_{MT}. The MT deployment height is regulated by the control variable u. A_{MT} and B_{MT} are respectively the MT model state and control matrices. More details about the dynamic model of MT and the state matrix coefficients can be found in the work of Macquart *et al.*[29]

4.2. TRAILING EDGE FLAP

The TEF aerodynamic response model is based on the work of Leishman.[31] The TEF model also called indicial model, assuming thin aerofoil and attached flow, describes the TEF dynamics in a linear state space form as follows:

$$\dot{\vec{X}}_F = A_F\vec{X}_F + B_F u \tag{8}$$

$$\dot{\vec{X}}_F = \begin{bmatrix} 0 & 1 & 0 \\ a_F & b_F & c_F \\ 0 & 0 & \tau_f \end{bmatrix} \vec{X}_F + \begin{bmatrix} 0 \\ 0 \\ 1 \end{bmatrix} u \tag{9}$$

$$\vec{X}_F = \begin{bmatrix} z & \dot{z} & \delta_F \end{bmatrix}^T \tag{10}$$

$$\Delta C_L = C_{\Delta C_L}\vec{X}_F = \begin{bmatrix} c_{F1} & c_{F2} & c_{F3} \end{bmatrix}\vec{X}_F \tag{11}$$

where, in the state vector, $\vec{X}_F$, δ_F and z respectively denote the TEF position and the aerodynamic state variable. The model parameters are given in Table I.$b_{F1,F2}$ and $A_{F1,F2}$ represent the exponents and coefficients of the function used to approximate the Wagner function. In addition, b_F is the semi-chord ($c/2$) and e is the flap hinge location expressed in terms of semi-chord. The F_i terms represent geometric parameters depending on the relative size of the flaps with respect to the aerofoil chord. For more details on the aerodynamic model, see Leishman, 1994.[31] The net lift increase because of the aerodynamic response of a deploying TEF is shown in Figure 5.

In this study, the TEF aerodynamic model is a reduced version of Leishman's original model. The original model includes the TEF deployment speed and acceleration contributions to the generated lift. However, for low-frequency applications (i.e. <10 Hz) such as the vibration of large blades, the lift contribution attributed to the TEF motion is negligible compared with the contribution from the TEF position and the aerodynamic state variable. This is illustrated in Figure 6 where we compare the responses of the original and reduced models when the TEF is set to deploy at frequencies of 10 and 50 Hz.

The TEF model may lose accuracy when employed for applications where the assumptions of attached flow and thin aerofoils are not always satisfied (e.g. wind turbine blades). In order to increase the accuracy of the steady state lift, we propose to introduce a new dependent parameter defined as $P_1(\alpha)$ in the lift matrix (11) as follows $C_{\Delta C_L} = \begin{bmatrix} P_1 c_{F1} & c_{F2} & c_{F3} \end{bmatrix}$. The position of $P_1(\alpha)$ is chosen such that it modifies the linear steady state slope of ΔC_L by varying the contribution of the aerodynamic state variable z without modifying the system dynamic. An optimization algorithm is then used to find $P_1(\alpha)$ such that the root mean square error between the model and XFoil[32] results are minimized. A comparison between the original, modified models and XFoil results is shown in Figure 7.

Table I. TEF aerodynamic model coefficients.

Matrix A_F coefficients	Matrix C_F coefficients
$\tau_F = -10$	$c_{F3} = F_{10}$
$c_F = F_{10}/\pi$	$c_{F1} = \pi b_{F1} b_{F2} (V_{rel}/b)^2$
$a_F = -b_{F1} b_{F2} (V_{rel}/b_F)^2$	$c_{F2} = 2\pi (A_{F1} b_{F1} + A_{F2} b_{F2})(V_{rel}/b)$
$b_F = -(b_{F1} + b_{F2})(V_{rel}/b_F)$	

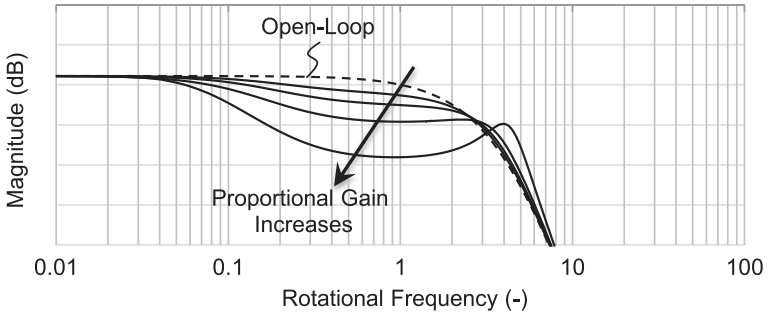

Figure 6. Original and reduced TEF models when deploying at frequencies of (a) 10 Hz and (b) 50 Hz.

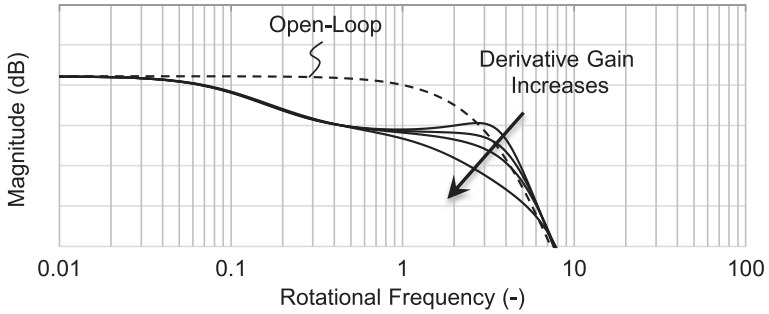

Figure 7. Comparison between the steady state of the different aerodynamic models of TEF when equipped on the S808 aerofoil and for an angle of attack of 15°.

5. A WIND TURBINE CASE STUDY

As previously mentioned, the proposed methodology considers wind turbine blades operating in attached flow conditions. In particular, this research work focuses on large operating under normal conditions. Since wind turbine blades are subject to rotational effects and experience highly turbulent wind fields, a modern multi-megawatt wind turbine is chosen as a case study.

The wind turbine model used for this investigation is the variable speed, pitch-controlled 5 MW wind turbine described in the work of Jonkman *et al.*[33] The main wind turbine characteristics are summarized in Table II. The performance and limitations of MTs and TEFs equipped on the National Renewable Energy Laboratory (NREL) 5 MW wind turbine blades are presented in Table III. The layout adopted for this study is illustrated in Figure 8. This CS layout is chosen as the result of a known trade-off between aerodynamic efficiency and structural requirement. That is, CSs should generally be placed far along the blade span in order to increase their load alleviation capabilities[34] but far enough from the tip in order to be able to fit the deployment mechanism inside the blade. Furthermore, complex aerodynamic phenomena occurring at the blade tip may also be avoided by not locating the controls surface close to the tip.

The unsteady results presented in the following sections are based on unsteady wind field generated utilizing TurbSim.[35] The generated wind fields used for this study are based on the von-Karman turbulence model according to the IEC 61400-3 standard and 'type A' turbulences. Unsteady simulations are carried out for the discrete mean wind speed values of 10, 13, 15, 18 and 22 m s^{-1} in order to determine the effect of mean wind speed on the behaviour of the proposed control strategy. The effect of the yaw angle is not investigated, and the yaw angle is therefore set to zero.

Table II. Wind turbine general features.

General characteristics	Hub height	87.6 m
	Diameter	126 m
	Blade length	61.5 m
	Blade mass	17,740 kg
	Number of blades	3
	Rated speed	12.1 rpm
	Blade structural damping (in % of critical damping)	<3%
Blade natural frequencies[23]	1st Flapwise	0.7056 Hz
	2nd Flapwise	2.0088 Hz
	1st Edgewise	1.0943 Hz
	2nd Edgewise	4.0918 Hz

Table III. Control surfaces features.

	Trailing edge flap	Microtab
Covered span (in percent of radius)	20%	20%
Locations (in percent of radius)	70–90%	70–90%
Size (in percent of chord)	10%	≈1% and 2%
Maximum deployment	±10°	±1 (normalized)
Maximum deployment speed	$\pm 100° \, s^{-1}$	±10 s (normalized)
Maximum lift generation ΔC_L	≈0.38	≈0.17

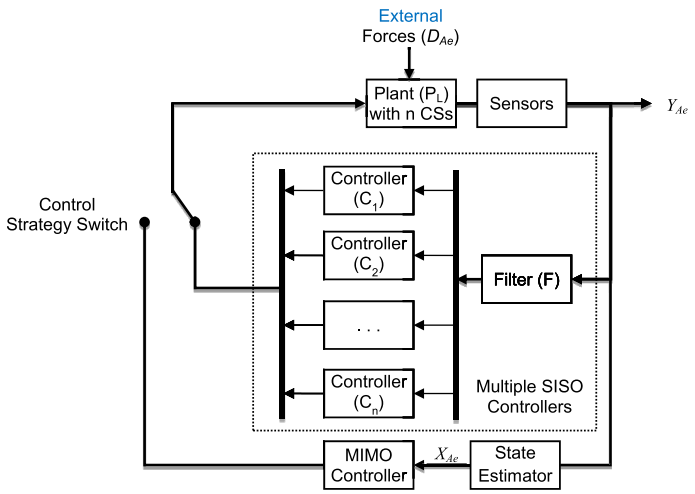

Figure 8. Illustration of a wind turbine blade equipped with CSs, a strain gauge sensor and Pitot tubes.

Figure 8 shows the blade equipped with a strain sensor located at 15% of the blade span. Strain gauges are commonly used in wind turbine applications in order to measure strains resulting from the action of external forces. After noise filtering, either strain measurements can be used directly as feedback data for the control system or moments and loads can be calculated.[26] Regardless of the chosen measurement signal, the blade frequency responses will have similar shapes because of the strong correlation between the strain measurements and the blade moments. As a result, both methods are therefore suitable for the proposed approach since only the shape of the Bode plot is of interest when designing a loop-shaping controller. During our study, the blade displacement frequency response due to the generalized modal forces is used. While generalized modal forces cannot be directly measured, a close correlation between the first modal forces and the blade moments is assumed since both moments and the generalized modal forces are linear combinations of distributed forces along the blade span.

Each blade is also equipped with two 5-hole Pitot tubes. The Pitot tubes are located at the ends of the CSs string as shown in Figure 8 and are used to estimate the local angles of attack and flow velocities.[23] This is necessary in order to update the aerodynamic CS models that are dependent on local flow velocity as shown in Table I.

5.1. CONTROLLERS

Two of the most common control structures employed in the literature, namely, the PID and the LQR are employed. The PID controller is the classical control structure that will be used with the loop-shaping approach. On the other hand, the LQR controller will be used as reference to evaluate the efficiency of the proposed loop-shaping control strategies. Load alleviation employing LQRs have been proposed in several studies.[9,26] In general, the control feedback consists of a linear combination of weighted signals as shown in equation (12). These signals represent the magnitudes of frequency bandwidths (F_{bi}) to be rejected. By applying different weights (w), specific frequency loads can be alleviated. The criterion may also consider the actuation of CSs.[9]

$$u = \min \int_{t0}^{tf} w_1 F_{b1} + w_2 F_{b2} + \ldots + w_n F_{bn} dt \tag{12}$$

It should be noted that in this paper the observability of aerodynamic surfaces equipped with CSs is not investigated. The state space vector is assumed fully known for the implementation of the LQR. This assumption is made to maintain focus on the loop-shaping analysis rather than into the details of the state estimation and observer design.

5.2. NUMERICAL TOOL

The wind turbine aeroelastic simulation is carried out using Wind Turbine Aeroelastic and Control[23] (WTAC). An FE code is used in WTAC in order to model the wind turbine blades as rotating tapered beams using the blades cross-sectional properties as input.[33] The blade structural model is also dynamically coupled to an aerodynamic blade element momentum code. In WTAC, the coupled edgewise and flapwise dynamics due to structural twist are described using twisted mode shapes as shown in Figure 9. The out-of-plane and in-plane axes are used as general blade coordinate systems. More details and validations about WTAC can be found in the work of Macquart and Maheri.[23] In general, it has been demonstrated that wind turbine blade dynamics can be well approximated by as few as two to three modes.[9,27] The first three modes are used in the rest of this study.

5.3. FREQUENCY-BASED CONTROL DESIGN

The impacts of control system designs on the dynamics of wind turbine blades equipped with CSs (blade–CSs) are now investigated. This section is divided into the *simplified*, the *individual CS* and the *multiple CS* frequency control analyses.

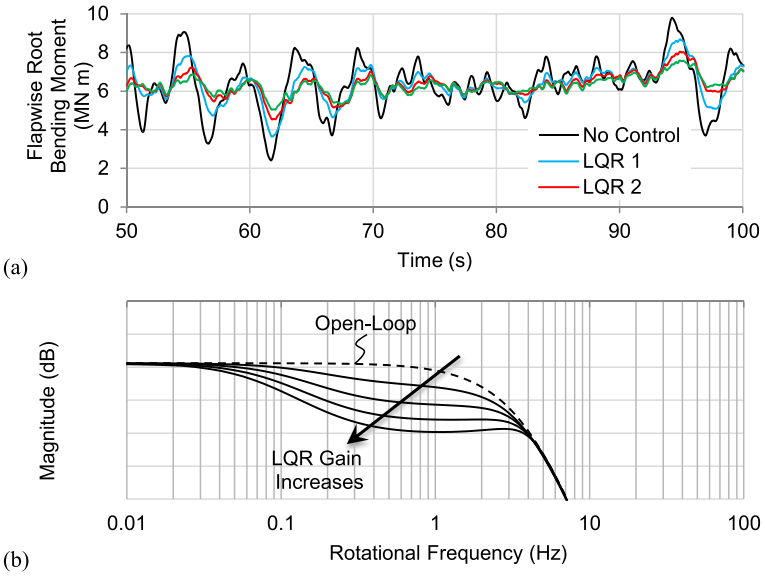

Figure 9. NREL 5 MW wind turbine blade coupled in-plane (IP) and out-of-plane (OOP) mode shapes (MS) as function of the normalized radial coordinate (r^*) models.

For the sake of simplicity, the load alleviation on wind turbine blades equipped with CSs is first studied without considering the CSs deployment and speed constraints. These constraints are taken into account later for the quantitative evaluation presented in Section 5.4.

5.3.1. Simplified frequency control analysis.

The simplified frequency control analysis is proposed in order to gain insights into the dynamic of the blade–CSs system based on a simplified analogous model. The following assumptions are made:

Assumption i. Blades equipped with multiple CSs are assumed to be dynamically equivalent to blades equipped with a single CS. This follows from the aerostructural matrix of wind turbine blades equipped with multiple CSs (equation (3)), in which each CS independently impacts the blades' structural dynamic. This assumption permits writing the aerostructural system in a SISO form for which the frequency analysis is simplified.

Assumption ii. In WTAC, the aerodynamic damping results from the feedback of the velocity of the blades' structural deformation to the aerodynamic module. In order to include the aerodynamic damping in the model used for the frequency analyses, a virtual damping proportional to the structural deformation velocity[36] is added to the structural model of equation (3) in order to obtain a stand-alone aerostructural model. This stand-alone aerostructural model is simply the combination of the non-rotation blade model with the added damping terms used to represent aerodynamic damping. This model is blade based, and all the rotating terms appearing in generalized model are, in our case, all included into the external forcing terms. A comparison between WTAC and the stand-alone aerostructural model calculation is shown in Figure 10.

Resulting from Assumption (ii), Figure 11 shows the frequency response of the structural and the aerostructural (i.e. with aerodynamic damping) blade models. As observed in this figure, the aerostructural model dynamic, because of the substantial amount of aerodynamic damping, is analogue to a low-pass filter dynamic. While this is a simplification achieved because of the significant aerodynamic damping value used, the proposed control approach could also be carried out for less damped systems. The simpler model is only chosen for the sake of clarity.

Based on the aforementioned assumptions, the simplified frequency analysis is now carried out. Filtering the output measurement (Y_{Ae} in Figure 2) such that the filtered signal contains all frequencies to be alleviated (i.e. reference set to zero), the closed-loop control structure can be redrawn as in Figure 12. The external forces are viewed as inputs, and the controller and filter are located in the feedback loop.

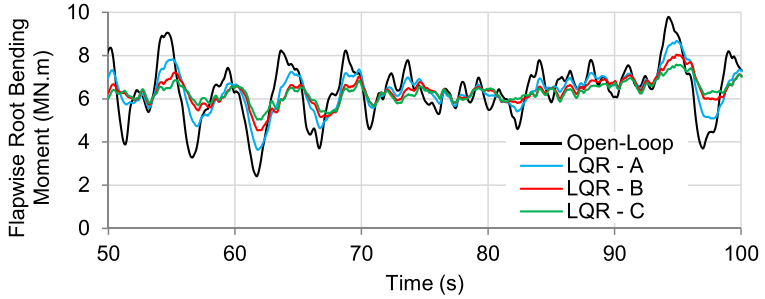

Figure 10. Flapwise root bending moment predicted by WTAC and the stand-alone aerostructural wind turbine blade model for a mean wind speed of 13 m s^{-1}.

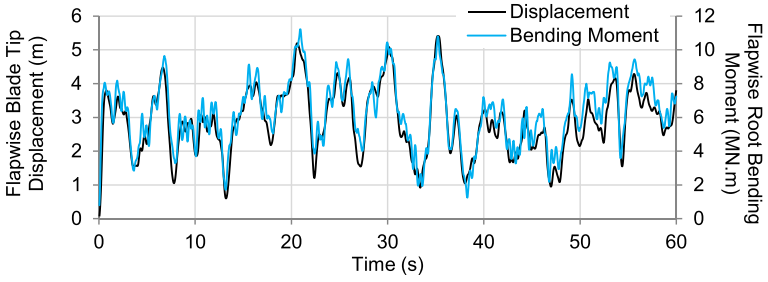

Figure 11. Typical frequency response of the non-rotating structural and aerostructural wind turbine blade

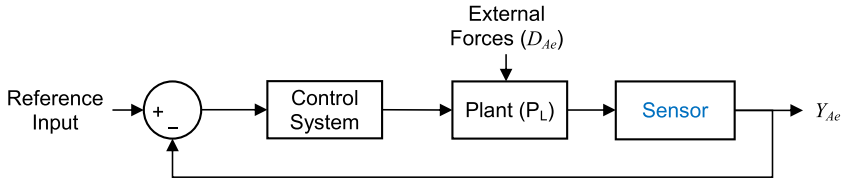

Figure 12. SISO closed-loop control structure for wind turbine blades equipped with CSs (reference set to zero).

Utilizing the analogous single-order low-pass filter model resulting from Assumption (ii), the closed-loop transfer function illustrated in Figure 12 is given as follows:

$$H_{cl} = \frac{Y_{Ae}}{D_{Ae}} = \frac{P_L}{1 + P_L CF} \tag{13}$$

Employing a P controller (i.e. K_P gain) with a high-pass filter, the closed-loop system equation becomes

$$H_{cl} = \frac{P_L}{1 + P_L CF} = \frac{P_L}{1 + P_L K_p \frac{s}{s+\gamma_{\text{filt}}}} \tag{14}$$

where γ_{filt} stands for the filter dynamic parameter. The magnitude plots of the open-loop and closed-loop systems are presented in Figure 13. The simplified frequency analysis shows that the trivial combination of a P controller and a high-pass filter can be used to shape the plant frequency response for load reduction purposes. This procedure is now applied to the wind turbine blade aerostructural model equipped with a single CS (i.e. SISO case).

5.3.2. Individual control surface—frequency control analysis.

Figure 14 shows the magnitude plot of the blade–CS system equipped with the same control system (i.e. equation (14)). As this figure shows, a similar behaviour to the simplified frequency analysis is observed. That is, as the proportional gain increases, the alleviation of the rotational frequencies load increases. In addition, a shift and amplification of the natural frequency is observed because, in comparison with the single-order low-pass filter, the blade–CS system becomes unstable as the proportional gain increases.

In order to increase the closed-loop system stability, a derivative controller is added to the closed-loop control as shown in Figure 15. The derivative gain increases the virtual damping and therefore reduces the excitation of the blade natural frequencies.

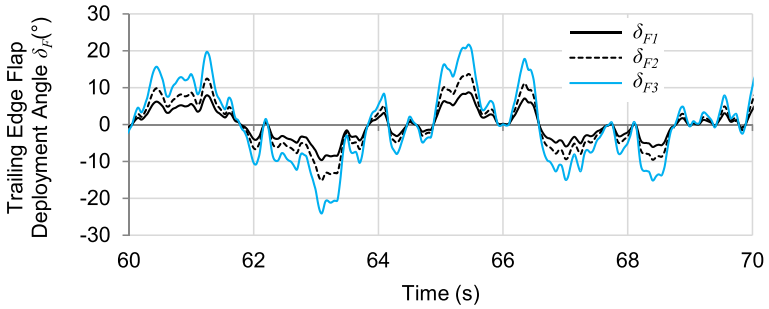

Figure 13. Bode plot of the open-loop and closed-loop low-pass filter.

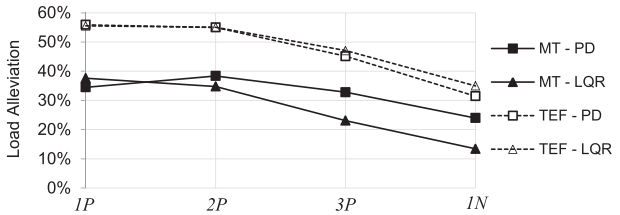

Figure 14. SISO wind turbine blade closed-loop dynamic response at mean wind speed of 15 m s^{-1} (P controller with a high-pass filter —pole at 0.3 rad s^{-1}).

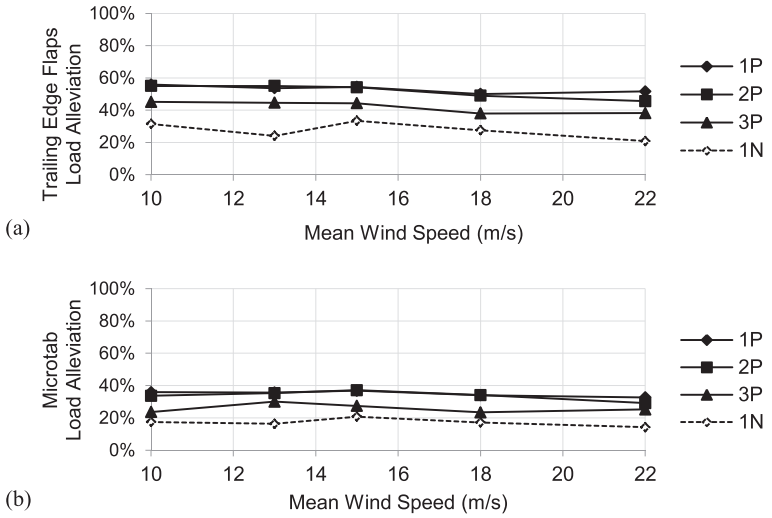

Figure 15. SISO wind turbine blade closed-loop dynamic response at mean wind speed of 15 m s^{-1} (PD controller with a high-pass filter—pole at 0.3 rad s^{-1}).

The aforementioned results show that the loop-shaping control method used for the simplified frequency analysis can also be successfully applied to a wind turbine blade equipped with a single CS. These results suggest that a feedback control consisting of a PD controller and a high-pass filter may be one of the simplest yet most effective control strategies for the SISO load alleviation of wind turbine blades.

5.3.3. Multiple control surfaces frequency control analysis.

So far, the control analyses were limited to SISO cases. However, wind turbine blades may be equipped with many CSs. In which case, we represent the control structure as in Figure 16. Here, the chief advantage of MIMO controllers is evident. The classical controllers form a repeated SISO control structure where each controller (C_1, …, C_n) must be tuned individ-ually. On the other hand, the MIMO controller calculates the deployment of all CSs in a straightforward manner while taking the overall system dynamic into account.

In this multiple CS case, the loop-shaping control using the classical SISO controller remains identical to the one presented in the previous sections. That is, the control of each CS is based on equation (14) and the interaction between CSs is assumed negligible. In comparison, the LQR criterion of equation (12) is designed to weigh the filtered output Y_{filt} of the augmented (subscript A) wind turbine blade model:

$$X_A = \begin{bmatrix} Q_2 & Q_1 & \dot{Q}_2 & \dot{Q}_1 & X_{Fc} & Y_{filt} \end{bmatrix}^T \tag{15}$$

$$A_A = \begin{bmatrix} 0 & 0 & 1 & 0 & 0 & 0 \\ 0 & 0 & 0 & 1 & 0 & 0 \\ r_2 & 0 & s_2 & 0 & [T_{As2}] & 0 \\ 0 & r_1 & 0 & s_1 & [T_{As1}] & 0 \\ 0 & 0 & 0 & 0 & [A_{Fc}] & 0 \\ 0 & 0 & c_{11} & c_{12} & 0 & \gamma_{\text{filt}} \end{bmatrix} \tag{16}$$

where the linear combination of c_{11} and c_{12} multiplying the modal coordinate derivatives represent the system output derivatives. For preliminary comparison, the LQR control strategy is evaluated for a wind turbine blade equipped with a single CS (i.e. SISO case). The magnitude plot and flapwise root bending moment of the blade–CS system are shown in Figure 17. The criterion weight is increased 10-fold between LQR 1 and LQR 2 and LQR 2 and LQR 3. As can be seen, the magnitude plot of the LQR shows obvious similarities with the PD controller Bode plot of Figure 15.

The LQR control strategy is now applied to a wind turbine blade equipped with multiple CSs, and the load alleviation results are presented in Figure 18. The criterion weight is increased 10-fold between LQR-A and LQR-B and LQR-B and LQR-C.

As illustrated in Figure 18, the flapwise root bending moment alleviation using the MIMO controller is comparable with the one achieved for the SISO case of Figure 17(a). This can be explained as follows. When employing classical SISO

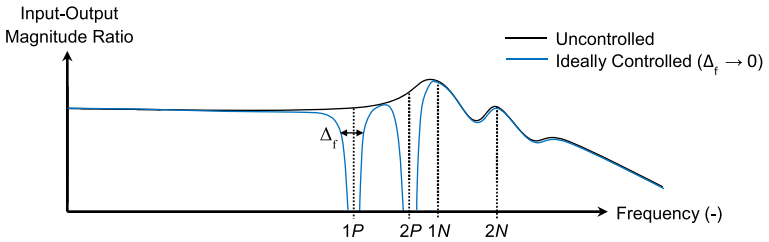

Figure 16. Control structures of a wind turbine blade equipped with multiple CSs.

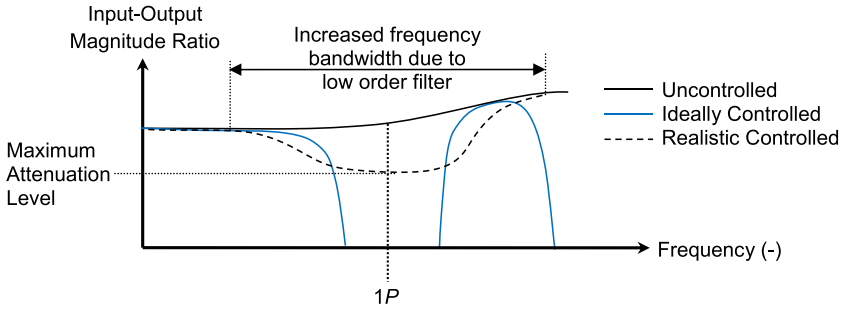

Figure 17. SISO wind turbine (a) blade flapwise root bending moment and (b) magnitude plot employing the LQR at mean wind speed of 15 m s^{-1}.

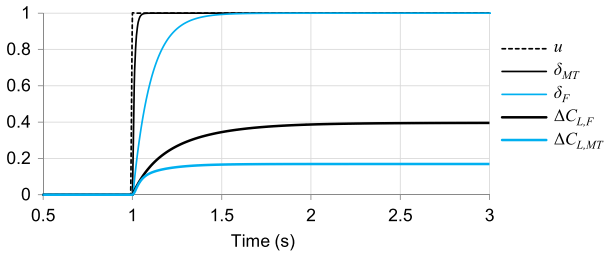

Figure 18. MIMO wind turbine blade flapwise root bending moment employing the LQR for a mean wind speed of 15 m s^{-1}.

controllers with a single reference signal (i.e. Y_{Ae} in Figure 16), all controlled CSs will deploy in-phase. By contrast, a MIMO controller such as the LQR is able to control each CS independently. However, flapwise measurements made over the whole blade span are strongly correlated as shown in Figure 19. This figure overlaps the blade tip displacement with its root bending moment. These two signals, taken as far apart as possible along the blade span, show a strong correlation.

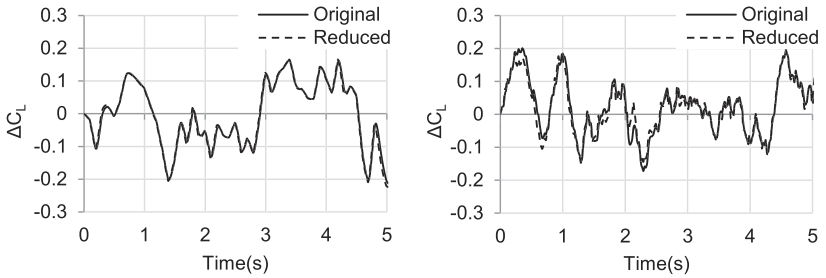

Figure 19. Superposition of the NREL 5 MW wind turbine blade flapwise tip displacement and root bending moment for a mean wind speed of 15 m s^{-1}.

Consequently, the deployment of TEFs controlled using the LQR are also in-phase with each other as shown in Figure 20. In other words, the deployment of multiple CSs, implemented anywhere along the blade of the NREL 5 MW wind turbine follows a deployment pattern imposed by the dominant vibrating mode. Moreover, this deployment pattern fixed irrespectively of the controller used.

The prime conclusion of this section follows: the dominant vibrating mode and the limited control capabilities and interactions between CSs are such that the original MIMO control problem can 'effectively' be decoupled into SISO control problems. Note that the MIMO control problem has not been mathematically decoupled but the particularities of this vibration problem permits to assume an 'effective' decoupling. Furthermore, considering the monotonic nature of the dominant vibrating modes throughout the entire blades, the proposed decoupling should also be effective for any flap configurations.

5.4. LOAD REDUCTION QUANTITATIVE RESULTS

In this section, a quantitative assessment of the load alleviation performance employing multiple CS on the NREL 5 MW wind turbine blades is carried out. In comparison with the results presented in Section 5.3, the physical limitations such as MTs and TEFs maximum deployment height and angle as well as maximum deployment speeds are considered according to Table III. The NREL 5 MW wind turbine blades are equipped with CSs covering 12 m or 20% of the blade span from 44.5 to 56.5 m.

In order to encompass the broad frequency content of aerodynamic loads, simulations are carried out for 10 min. Since loads are spread over frequency bandwidths, the load alleviation is calculated by averaging the load reduction in separate intervals centred at the rotational and natural frequencies as follows[23]:

$$LA = 100\left(\frac{\sum_{nP-\mu}^{nP+\mu}\left(f_{noc}(\omega) - f_c(\omega)\right)}{\sum_{nP-\mu}^{nP+\mu} f_{noc}(\omega)}\right) \tag{17}$$

in which $f_{noc}(\omega)$ and $f_c(\omega)$ respectively denote the flapwise root bending moment frequency spectrum for the uncontrolled and controlled case and $[nP-\mu\ ,\ nP+\mu]$ is the interval over which the results are averaged for the first, second and third rotational frequencies ($n=1,\ 2$ and 3) as well as the first natural frequency. A 10% frequency range is chosen in this study.

Because of the MT and TEF aerodynamic model similarities (Section 4), similar results were found for both CSs. For the sake of clarity, the TEF results employing the PD control strategy based on the loop-shaping approach are presented first as in Table IV. According to equation 19, a positive percentage denotes a load reduction, while a negative percentage refers to

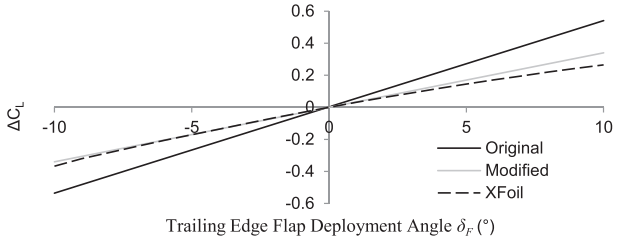

Figure 20. Unconstrained TEF deployment angle (δ_F) according to the MIMO LQR control strategy.

Table IV. Load alleviation of the NREL 5 MW wind turbine employing TEF (loop-shaping multiple SISO PD controller, 10 m s^{-1} turbulent wind).

	$K_p=-500\ K_d=200$	$K_p=-250\ K_d=200$	$K_p=-250\ K_d=0$
1*P*	55.89%	51.11%	58.06%
2*P*	55.02%	56.65%	46.36%
3*P*	45.15%	50.46%	14.25%
1*N*	31.48%	40.45%	−19.19%

an increased load excitation. It can be observed that the multiple SISO control results of wind turbine blade presented in Table IV are in complete agreement with the frequency analyses of Section 5.3. That is, when the derivative gain is set to zero, the maximum 1*P* load alleviation occurs and an amplification of higher frequency loads is observed as expected from the results presented in the frequency analysis section (i.e. Figure 15). When the derivative term is used, the 1*P* load alleviation decreases, while the load alleviation spans a greater frequency bandwidth (i.e. up to 1*N*).

The load alleviation results comparing the best found MTs and TEFs SISO and MIMO controllers for the NREL 5 MW wind turbine operating in an unsteady wind field of 10 m s^{-1} mean wind speed are presented in Figure 21. As expected, TEFs have a greater control space and therefore show higher load alleviation performance compared with MTs. Similar performance in easing 1*P* loads are observed regardless of the controller used (i.e. LQR and PD). This can be explained as follows: the 1*P* counteracting loads to be generated by the string of CSs are greater than the CSs reachable space (maximum achievable moment by the string of CSs) and consequently all CSs deploy to their maximum value.

Figure 21 also shows that the load alleviation results achieved with the multiple PD SISO control loops and the LQR MIMO control strategy are comparable. A high load alleviation percentage is observed for 1*P* and 2*P* loads, and the load alleviation percentage is shown to decrease as the frequency of loads increases. This is in agreement with results presented by Rice and Verhaegen,[21] which showed that it becomes increasingly difficult for CSs to alleviate loads as their frequencies increase. The PD and LQR load alleviation of 3*P* and 1*N* frequency loads show some discrepancies likely because of different tunings and rates at which the CSs are activated. Faster actuations allow for more 1*N* load alleviation but wear more on the CSs actuators.

Finally, Figure 22 shows the TEFs and MTs PD controller load alleviation results as functions of the wind fields mean wind speeds. It can be observed that the PD control structure used with the multiple SISO loop-shaping approach shows to be relatively robust to change in operating conditions. The nearly constant load alleviation ratio achieved in the presented study can be explained as follows. The flap lift coefficient remains nearly constant in the linear aerodynamic region. Hence, flap lift generation will also increase as the local flow velocity increases. In other words, as the mean wind speed increases, both turbulent load and flap load alleviation will increase.

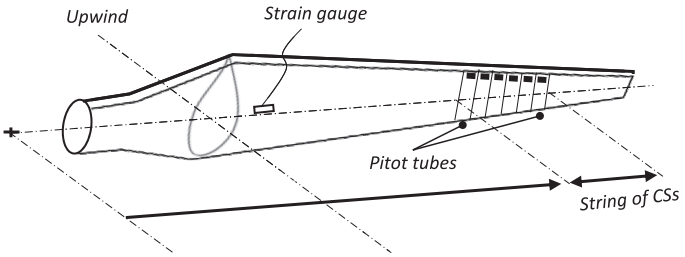

Figure 21. Best found load alleviation controllers for the NREL 5 MW wind turbine (mean wind speed of 10 m s^{-1}).

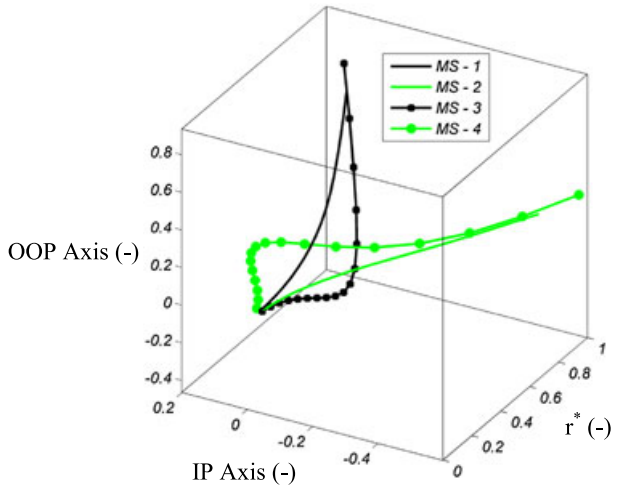

Figure 22. Load alleviation performance of (a) TEFs and (b) MTs as a function of the turbulent wind field mean wind speed.

6. SUMMARY OF RESULTS

This investigation provides an in-depth control analysis for the load reduction of wind turbine blades subject to external forces while employing CSs. A frequency-based approach was used to successfully explain the closed-loop system dynamic of actively controlled wind turbine blades. The results of this research are summarized as follows:

1. The deployment of multiple active flow controllers on wind turbine blades was shown to follow a pattern imposed by the dominant vibrating mode. Moreover, this pattern or mode shape is monotonic throughout the blade span.
2. The MIMO control problem of wind turbine blades equipped with multiple active flow controllers can be 'effectively' decomposed into simpler decoupled SISO control problems.
3. The proposed classical SISO control systems were shown to be highly efficient at reducing the aeroelastic vibrations of wind turbine blades employing CSs.
4. For this particular case study, both CSs were shown to be capable of alleviating loads up to the first blade flapwise natural frequency. In particular, significant 1*P* load alleviation was demonstrated. While the load alleviation quantification results are very promising, more advanced models and extensive work is required in order to obtain more realistic results.

In the case where CS would cover a larger extent of the blade span, this paper's main conclusion (1 and 2) will hold true. Wind turbine blade dynamics are dominated by the few first modes. This trend is likely to continue as blades are becoming larger. As a result, the correlation between actuator deployment and structural dynamic will remain strong along the blade span. This is also true for the aerodynamic behaviour of flaps for variable speed pitch-controlled wind turbine blades that maintain the majority of the blade span in the linear aerodynamic region. As a result, the conceptual decoupling approach presented in this paper can be applied to simplify the wind turbine blade load alleviation problem as long as CSs are located along the linear aerodynamic region of the blade span.

REFERENCES

1. Staino A, Basu B, Nielsen Søren RK. Actuator control of edgewise vibrations in wind turbine blades. *Journal of Sound and Vibration* 2012; **331**: 1233–1256.
2. Li D, Guo S, Xiang J. Aeroelastic dynamic response and control of an airfoil section with control surface nonlinearities. *Journal of Sound and Vibration* 2010; **329**: 4756–4771.
3. Lim IG, Lee I. Aeroelastic analysis of rotor systems using trailing edge flaps. *Journal of Sound and Vibration* 2009; **321**: 525–536.
4. Weisshaar TA. Morphing aircraft systems: historical perspectives and future challenges. *Journal of Aircraft* 2013; **50**: 337–353.
5. Lachenal X, Daynes S, Weaver PM. Review of morphing concepts and materials for wind turbine blade applications. *Wind Energy* 2013; **16**: 283–307.
6. Veers PS, Ashwill TD, Sutherland HJ, Laird DL, Lobitz DW, Griffin DA, Mandell JF, Musial WD, Jackson K, Zuteck M. Trends in the design, manufacture and evaluation of wind turbine blades. *Wind Energy* 2003; **6**: 245–259.
7. Bossanyi EA. Individual blade pitch control for load reduction. *Wind Energy* 2003; **6**: 119–128.
8. Stanewsky E. Adaptive wing and flow control technology. *Progress in Aerospace Sciences* 2001; **37**: 583–667.
9. Castaignet D, Barlas T, Buhl T, Poulsen NK, Wedel Heinen JJ, Olesen NA, Bak C, Kim T. Frequency-weighted model predictive control of trailing edge flaps on a wind turbine blade. *IEEE transaction on control system technology* 2013; **21**: 4.
10. Bossanyi E, Savini B, Iribas M, Hau M, Fischer B, Schlipf D, Engelen T, Rossetti M, Carcangiu CE. Advanced controller research for multi-MW wind turbines in the UPWIND project. *Wind Energy* 2012; **15**: 119–145.
11. Cook RG, Palacios R, Goulart P. Robust gust alleviation and stabilization of very flexible aircraft. *AIAA Journal* 2013; **51**: 330–340.
12. Van Dam CP, Nakafuji DY, Bauer C, Chao D, Standish K. Computational design and analysis of a microtab based aerodynamic loads control system for lifting surfaces. *SPIE International Society for Optical Engineers* 2002.
13. Schubel PJ, Crossley RJ. Wind turbine blade design. *Energies* 2012; **5**: 3425–3449.
14. Song ZG, Li FM. Active aeroelastic flutter analysis and vibration control of supersonic composite laminated plate. *Composite Structures* 2012; **94**: 702–713.

15. Castaignet D, Barlas T, Buhl T, Poulsen NK, Wedel Heinen JJ, Olesen NA, Bak C, Kim T. Full-scale test of trailing edge flaps on a Vestas V27 wind turbine: active load reduction and system identification. *Wind Energy* 2014; **17**: 549–564.
16. Barlas TK, Wingerden W, Hulskamp AW, Kuik GA, Bersee HE. Smart dynamic rotor control using active flaps on a small-scale wind turbine: aeroelastic modeling and comparison with wind tunnel measurements. *Wind Energy* 2013; **16**: 1287–1301.
17. Song ZG, Li FM. Active aeroelastic flutter analysis and vibration control of supersonic beams using the piezoelectric actuator/sensor pairs. *Smart Materials and Structures* 2011; **20**: 055013.
18. Wilson DG, Resor BR, Berg DE, Barlas TK, van Kuik GAM. *Active Aerodynamic Blade Distributed Flap Control Design Procedure for Load Reduction on the UpWind 5 MW Wind Turbine*. : City, 2010.
19. Berg D, Wilson D, Resor B, Berg J, Barlas T, Crowther A, Halse C, House R. *System ID Modern Control Algorithms for Active Aerodynamic Load Control and Impact on Gearbox Loading*. : City, 2010.
20. Barlas TK, van Kuik GAM. *Aeroelastic Modelling and Comparison of Advanced Active Flap Control Concepts for Load Reduction on the Upwind 5 MW Wind Turbine*. : City, 2009.
21. Rice JK, Verhaegen M. Robust and distributed control of a smart blade. *Wind Energy* 2010; **13**: 103–116.
22. Barlas TK, van der Veen GJ, van Kuik GAM. Model predictive control for wind turbines with distributed active flaps: incorporating inflow signals and actuator constraints. *Wind Energy* 2012; **15**: 757–771.
23. Macquart T, Maheri A. Integrated aeroelastic and control analysis of wind turbine blades equipped with microtabs. *Renewable Energy* 2014.
24. Van Wingerden J, Hulskamp A, Barlas T, Marrant B, Van Kuik G, Molenaar DP, Verhaegen M. On the proof of concept of a 'smart'wind turbine rotor blade for load alleviation. *Wind Energy* 2008; **11**: 265–280.
25. Barlas, T., van Wingerden, J.-W., Hulskamp, A. and van Kuik, G. Closed-loop control wind tunnel tests on an adaptive wind turbine blade for load reduction. Proceedings of the 46th AIAA/ASME2008 (n.d.).
26. Castaignet D, Poulsen NK, Buhl T and Wedel-Heinen JJ. Model predictive control of trailing edge flaps on a wind turbine blade. 2011 American Control Conference (2011), 4398–4403.
27. Jonkman JM, Buhl M. *FAST User's Guide*. National Renewable Energy Laboratory: Golden, CO, 2005.
28. Macquart, T. and Maheri, A. Integrated aeroelastic and control analysis of wind turbine blades equipped with microtabs. *Renewable Energy*, 752015(n.d.), 102–114.
29. Macquart T, Maheri A and Busawon K. Microtab dynamic modelling for wind turbine blade load rejection. *Renewable Energy*, 642014(n.d.), 144–152.
30. Chow R and van Dam CP. Computational investigations of deploying load control microtabs on a wind turbine airfoil. American Institute of Aeronautics and Astronautics (2007).
31. Leishman JG. Unsteady lift of a flapped airfoil by indicial concepts. *Journal of Aircraft* 1994; **31**: 288–297.
32. Drela M XFOIL: an analysis and design system for low Reynolds number airfoils (1989).
33. Jonkman JM, Butterfield S, Musial W, Scott G. *Definition of a 5-MW Reference Wind Turbine for Offshore System Development*. National Renewable Energy Laboratory Golden: CO, 2009.
34. Macquart T, Maheri A, Busawon K. *A Simple Method to Determine the Optimal Location of Active Flow Controllers on Wind Turbine Blades*. IEEE: City, 2014.
35. Foley JT and Gutowski TG. TurbSim: reliability-based wind turbine simulator. IEEE international symposium on electronics and the environment (2008), 315–319.
36. Salzmann D, Van der Tempel J. *Aerodynamic Damping in the Design of Support Structures for Offshore Wind Turbines*. : City, 2005.